JOURNAL OF MATERIALS SCIENCE 23 (1988) 3214–3224

Study on surface cracking of alumina scratched by single-point diamonds

ZHANG BI, H. TOKURA, M. YOSHIKAWA
Department of Mechanical Engineering, Faculty of Engineering, Tokyo Institute of Technology, 2-12-1 Ookayama, Meguro-ku, Tokyo 152, Japan

Scratching experiments have been carried out on hot-pressed alumina by using single-point diamonds of conical shape (conical angle 85, 108, 128 and 65° and nose radius 1.6, 1.1, 1.9 and 45.0 μm, respectively). With an increase of the scratching depth, the material exhibits the following behaviour: macroscopic plastic deformation → scale-like cracking → cracking or chipping. Cracking or chipping is absent only if the groove depths are less than certain values which vary with the diamond shape. The crack penetration depth is approximately in proportion to the depth of cut. For a depth of cut less than 2 μm, the penetration depth of crack induced by the diamond of nose radius 45.0 μm is almost 8 times those produced by the other diamonds. For a depth of cut more than 2 μm, the former is more than twice the latter. The coefficients of pile-up increase as the depths of cut decrease.

1. Introduction

Fine ceramics are expected to be used as structural materials for machinery because of their strength at high temperature, anti-corrosiveness, heat resistivity and wear resistivity, etc. However, in applying fine ceramics to practical usage, machining has been a problem, which results from their hardness and brittleness. Grinding with a diamond wheel is generally carried out upon fine ceramics, but it is a plain fact that the shapes, distribution and knock-out of the grain edges on the grinding surface are usually not uniform, and in addition the grinding surface of the diamond wheel changes very complicatedly in the course of grinding. Therefore, to obtain finely ground surface layers of ceramics with stable characteristics is very difficult.

For this reason, studies have been widely carried out which are aimed at elucidating the grinding mechanism by performing a scratching experiment on fine ceramics with a single-point diamond, rather than by performing a grinding experiment. Swain [1] observed the surface microcracking above scratches in a number of brittle solids, such as sapphire and glass, by using a Vickers pyramid indenter. He found that the nature of the cracking was very similar to that occurring about a quasi-static pointed indenter. Kirchner and co-workers [2–5] scratched hot-pressed silicon nitride and glass plates by diamond points with varying degrees of flatness mounted on a wheel rotating at varying speeds. They investigated the mechanisms of fragmentation and damage penetration, and claimed that the damage penetration at low vertical loads was approximately proportional to the load, whereas at high load, the load dependence of the crack length was much greater. Imanaka *et al.* [6] directly observed chip removal processes during the grinding of glass–ceramics and several types of oxide ceramic by a micro-flash technique. They found that the chips were generally of a fragment type and were distinguished from those of ductile materials, and a part of chips was removed directly by the diamond grain, but a considerable part splintered out of the ceramic immediately after the grain passed over.

As mentioned above, there are some scratching experiments on ceramics by using a single-point diamond tool which simulate the ceramic grinding process, as well as a few researches on the formation mechanism of cracks and fractures on the surface layer. However, few scratching experiments have been performed which use a sharp single-point diamond and set the depth of cut as small as that in the practical grinding of fine ceramics.

In this paper, the authors used sharp conical diamonds to scratch alumina ceramics with a very small depth of cut. After scratching, the scratches on the alumina surface were observed with a scanning electron microscope (SEM), and the profiles of the scratches were also measured. Then by using a taper-polishing and fracture method, the cross-sections of the scratches were investigated and the crack penetration state of the surface layer was made clear. At the same time, a formation mechanism of cracks and fracture was proposed. In addition, a blunt-pointed diamond with nose radius 45 μm was also used for experiments in order to simulate the grinding process performed by a worn grinding wheel.

2. Experimental procedure

The ceramic used for the experiments was polycrystalline alumina which was fabricated by the authors using a hot-pressing method. The powder consisted of alumina of purity more than 99.5%; the sintering temperature was 1480° C and the pressure for sintering 40 MPa. The sintered alumina had density

0022–2461/88 $03.00 + .12

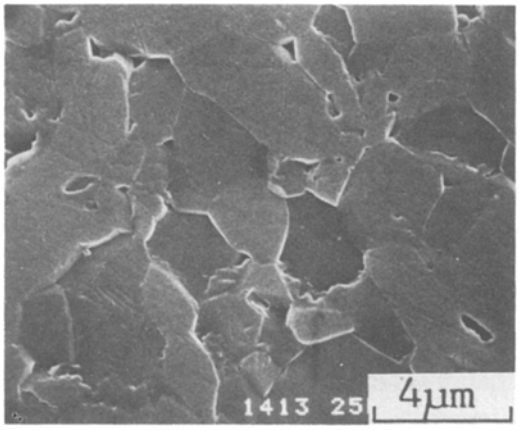

Figure 1 The microstructure of the alumina sample.

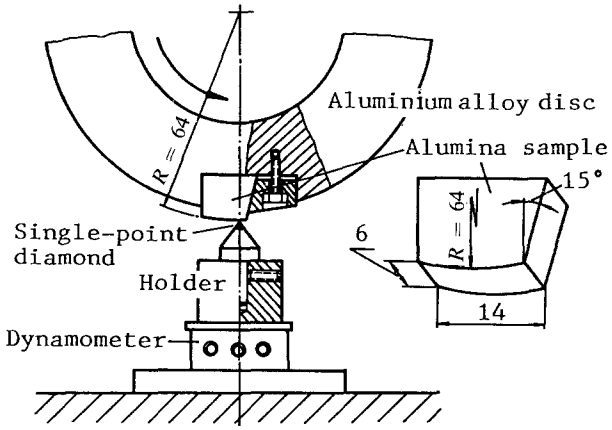

Figure 3 Geometry and dimensions of alumina sample and schematic arrangement of the scratching equipment. Dimensions in millimetres.

3.94 g cm^{-3}, bending strength 500 MPa, Vickers hardness 1830 and fracture toughness 5.3 MN m$^{-3/2}$. An SEM micrograph of the alumina is shown in Fig. 1. It can be seen from this picture that the alumina was well sintered with almost no pores.

A precision grinding machine with an aerostatic spindle and an aerostatic slider [7] was used for the scratching experiments. Fig. 2 shows the appearance of the machine. The alumina sample was shaped to the dimensions shown in Fig. 3. Before being shaped, the sample was chucked to the periphery of an aluminium alloy disc with a diameter 125 mm. Then, together with the disc, the sample was mounted on the aerostatic spindle. On the other hand, the single-point diamond was fixed on the aerostatic slider. In this kind of way, the depth of the scratched groove along the circumferential direction would remain unchanged. The scratching depth was set by a displacement sensor (Linear Inductosyn) with a resolution of 0.05 μm.

Fig. 4 shows an example of a single-point diamond used for the experiments. All the diamonds were examined with the SEM. Some parameters of the single-point diamonds are listed in Table I. In addition, stereographic projections of all these diamonds were obtained by means of the Laue back-reflection method. The crystal axes in the conical axis and the nose radii are also listed in Table I. Because the diamonds could not be classified systematically in conical angle, nose radius and conical axis, they were denoted only by their numbers. Table II shows the scratching conditions.

The surfaces around the scratched grooves were observed with the SEM, and sectional profiles of the scratched grooves were examined with a profile measuring machine which had a diamond feeler of tip radius 2 μm.

The crack observations were done by using a fracture method and taper polishing method as shown in Fig. 5. Fig. 5a gives a schematic description of the fracture method. The alumina sample was cut with a diamond grinding cutter from the bottom, and then broken down by a bending moment M. Cross-sections of the scratched groove on the fractured surface were observed with the SEM.

Fig. 5b shows a concept drawing of the taper polishing method. Alumina samples were first plated with copper and embedded in polyester resin. By using an ultra-precision polishing machine having a diamond polishing wheel, the sample was then aslant-polished out at an inclination angle of 35° to the scratched surface. This taper-polished surface was further lapped to a very smooth plane with 9, 6, 3 and 1 μm diamond pastes in turn. The scratched grooves lying on this taper surface were observed with the SEM, etched with 98% H_3PO_4 and then observed again.

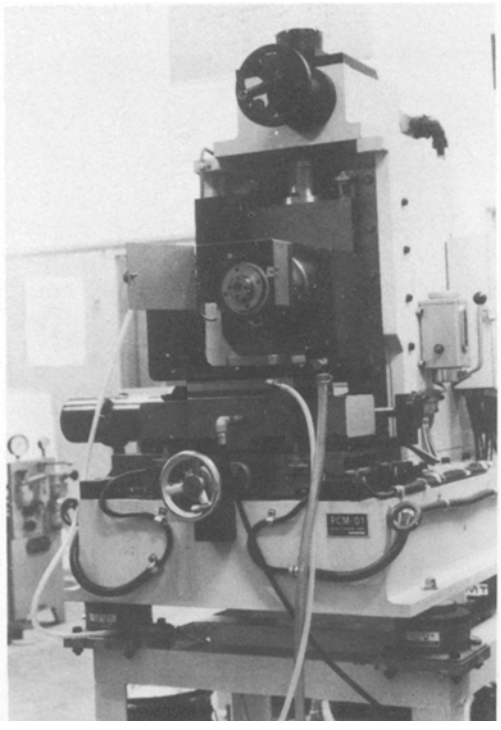

Figure 2 The appearance of the precision-grinding machine.

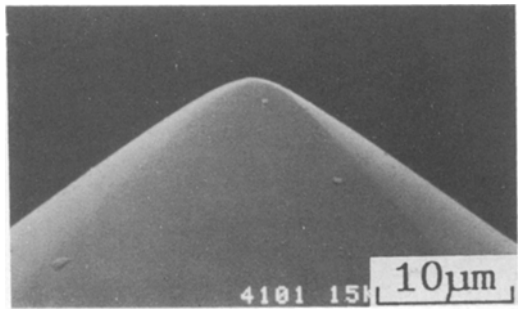

Figure 4 SEM observation of a single-point diamond.

TABLE I Some parameters of single-point diamonds used for scratching

Parameter	Diamond No.			
	1	2	3	4
Nose radius, R (μm)	1.6	1.1	1.9	45.0
Conical angle, θ (deg)	85	108	128	65
Crystal axis in conical axis	[1 0 0]	[1 1 0]	[1 0 0]	[1 1 1]

TABLE II Scratching conditions

Scratching speed	1600 m min^{-1}
Depth of cut	0 to 13 μm
Environmental conditions	Atmospheric
Coolant	None

3. Results and discussion

3.1. Surface cracking

Fig. 6 gives relations between the set depth and measured groove depth. As both of the depths agree with each other quite well over the whole range of the present depth of cut, the set depth of cut will be replaced by the groove depth from now on.

Fig. 7 shows surface views of the scratches formed by Diamond No. 1. The scratches are divided into four kinds corresponding to different depths of cut. In Fig. 7a the depth of cut was smaller than approximately 0.8 μm, the surface of the scratched groove was very smooth, almost no material removal occurred, and the groove appeared macroscopically to show a state of plastic deformation. In Fig. 7b the depth of cut was about 3.1 μm, some small cracks could be observed on the groove surface, but there was still no significant crack formation around the groove. Fig. 7c is the case with depth of cut 9.3 μm, the groove surface was rough, and cracking and small-scale chipping occurred on and around the groove. Fig. 7d shows the groove for 11.5 μm depth of cut; the cracks around the groove developed and induced a large-scale chipping. These grooves are sketched at the right-hand side.

As the depth of cut became larger, the scratched grooves changed in the following manner for different processes.

(a) *Macroscopic plastic deformation process.* In this process the depth of cut was very small, and there was almost no material removal. As the groove was compressed by the diamond, there was macroscopic plastic deformation of the surface layer. A part of the deformed material was forced to flow toward the two sides of the groove and formed a pile-up, while another part entered the pores at grain boundaries.

(b) *Scale-like cracking process.* For a depth of cut larger than in Process (a), not only was macroscopic plastic deformation formed, but also the material was removed as chips. Scale-like cracks formed on the bottom of the groove, which might be due to stick–slip events at the point of the diamond. The scale-like cracks would control the surface roughness on the groove bottom to some extent. In these experiments, this kind of scale-like crack appeared for depths of cut 1 to 3.5 μm. At these (a) and (b) stages, the grooved surface exhibited only plastic deformation on a macroscopic scale.

(c) *Cracking process.* When the depth of cut increased, the single-point diamond interfered deeply with the inside of the sample. A removal of material occurred, and cracks formed and developed radically from the groove. In this cracking process, the material

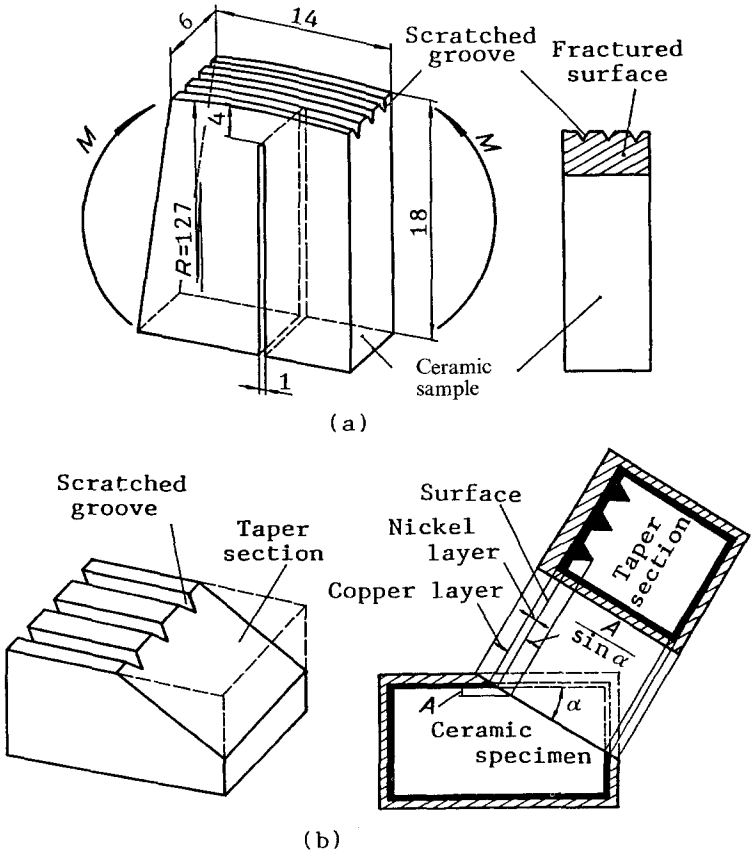

Figure 5 Schematic drawing for illustrating the fracture method and the taper polishing method. Dimensions in millimetres.

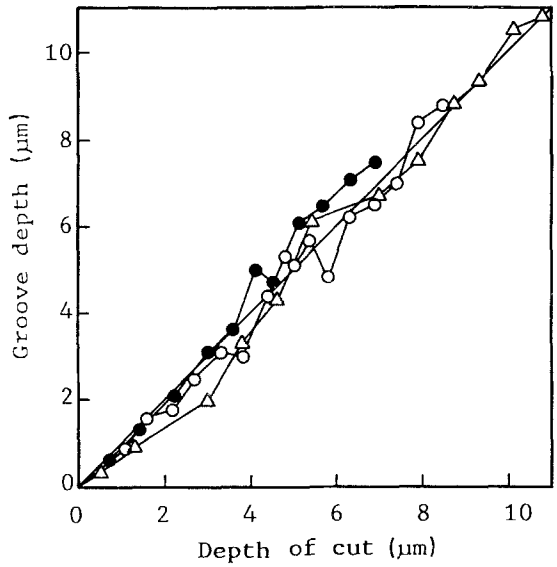

Figure 6 Groove depth against set depth for scratching with different diamonds (Table I): (△) No. 1, (○) No. 2, (●) No. 3.

showed brittleness. In the scratching experiments, the cracking process appeared for depths of cut 3.5 to 10 μm.

(d) *Chipping process.* When the depth of cut was large enough, the crack developed further and resulted in large-scale chipping and fragmentation. The material was to a large extent removed by chipping and fragmentation. In this chipping process, the material showed complete brittleness.

Scratched grooves were etched with 98% H_3PO_4. Fig. 8 shows the scratched grooves before and after etching. After etching, a 2 μm groove with a smooth surface became very coarse and rough, and a rough groove with 11 μm depth of cut was severely chipped. Because of this large-scale chipping, the macrocrack beneath the groove was clearly exposed.

The length of cracking or chipping in these processes was measured. The relations between the length and the groove depth are shown in Fig. 9. On this graph, one can see that the larger the conical angle or the nose radius of the diamond, the longer the length of cracking. The surface crack lengths increased with an increase of the groove depth. In the case of Diamond No. 4 which had a nose radius of 45 μm, the crack length reached about 95 μm, whereas the groove depth was only 9 μm. However, in the case of the other diamonds with nose radii 1.1 to 1.9 μm and conical angles 85, 108 and 128°, the surface crack lengths are approximately 30, 40 and 50 μm, respectively, at the same 9 μm groove depth.

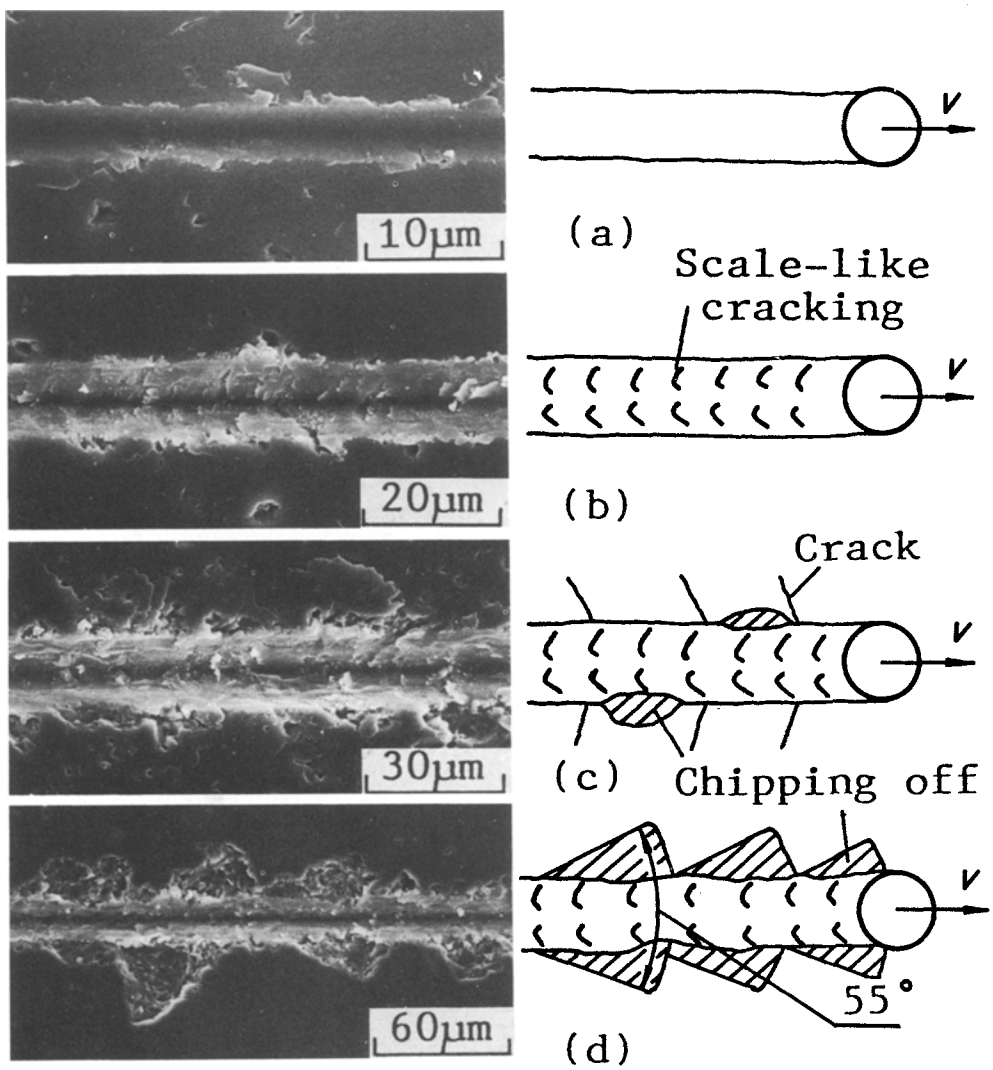

Figure 7 Views from above of scratches formed by Diamond No. 1 (R = 1.6 μm, θ = 85°). Arrows represent moving directions of diamond. (a) Smoothly ductile grooving, groove depth 0.8 μm; (b) coarsely ductile grooving, groove depth 3.1 μm; (c) cracking, small-scale chipping and grooving, groove depth 9.3 μm; (d) large-scale chipping and grooving, groove depth 11.5 μm.

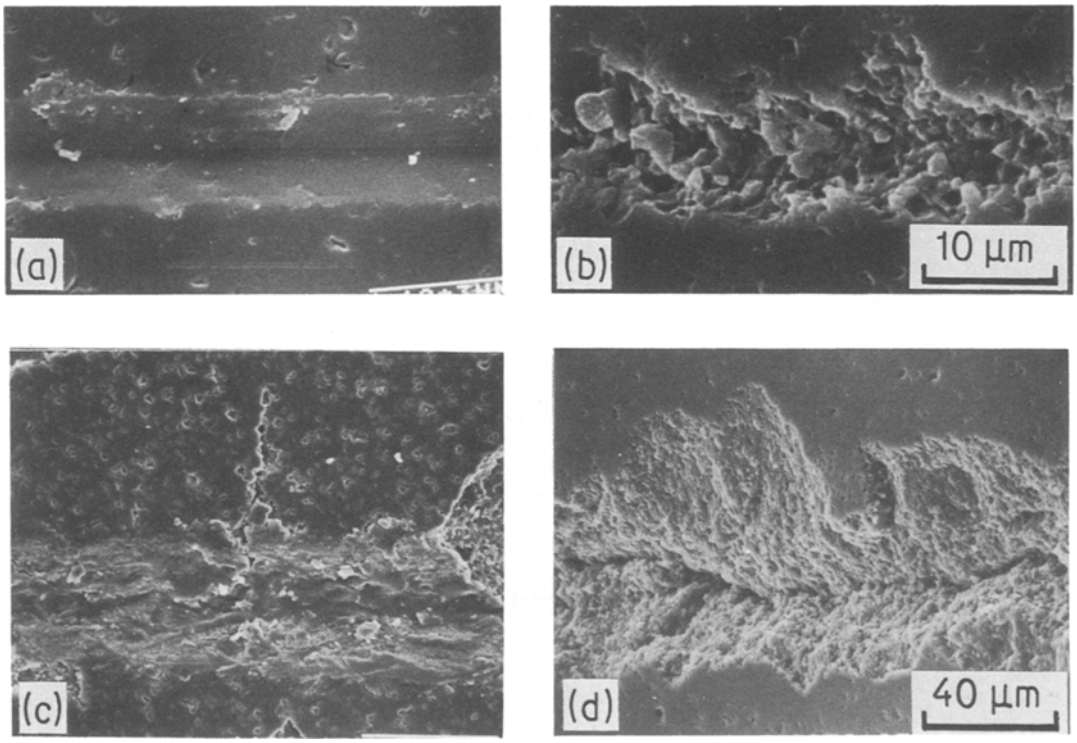

Figure 8 SEM observations of a smooth groove and a rough groove before and after etching. Scratching direction from left to right. Depth of cut 2 μm: (a) before, (b) after etching. Depth of cut 11 μm: (c) before, (d) after etching.

3.2. Pile-up around the scratched groove

Fig. 10 gives SEM observations of the grooves scratched by Diamond No. 4 and the transverse profiles of these grooves. The pile-up B tended to be higher as the groove depth A increased. When surface cracking occurred the pile-up was extremely high. The grooved sample was therefore sectioned and observed so as to elucidate the origin of the pile-up.

Fig. 11 shows cross-sections of the scratched grooves of 8.5 μm depth of cut using Diamond Nos 2 and 4. In both cases the pile-up formed on the two sides of the groove, and these pile-ups were due to the microcrack clusters beneath the groove surface. Thus, there existed microcrack clusters in the subsurface region of the grooves; these microcrack clusters resulted from scratching by the diamond, and appeared as if they were deformed plastically from the macroscopic point of view. It should be considered that this kind of microcrack cluster played an important role to the formation of the pile-up.

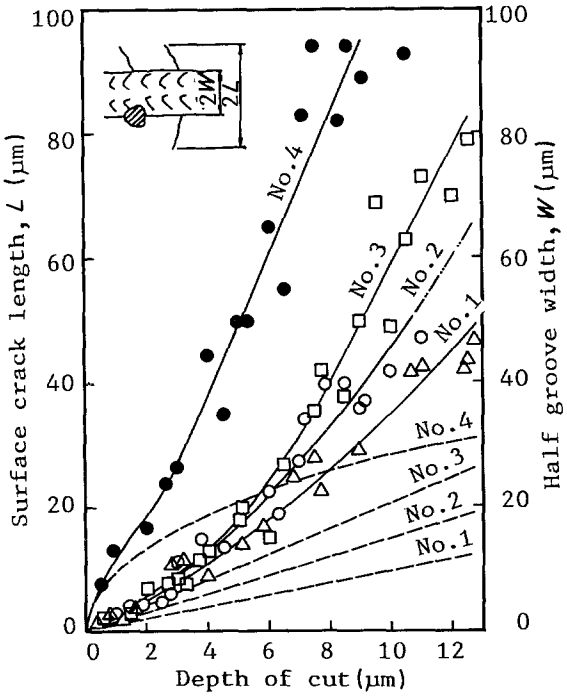

Figure 9 (——) Surface crack length and (– – –) half groove width against groove depth for single-point scratching.

The relation of the pile-up coefficient and the depth of cut are shown in Fig.12, where the maximum depth of cut was 3.5 μm. The reason for choosing 3.5 μm is that there was almost no cracking or chipping around the scratched grooves up to this depth of cut. Here, the ratio of the average height of the pile-up B to the groove depth A, B/A, is defined as the pile-up coefficient. Fig. 12 shows the fact that the smaller the depth of cut, the greater the pile-up coefficient. On the other hand, the pile-up coefficient with the larger nose-radius Diamond No. 4 was almost twice as large as those for the diamonds with nose radii 1.1 to 1.9 μm. In addition, in the latter case the diamonds with large conical angle produced large pile-up coefficients. The reason for this may be considered as follows.

In a given depth of cut, the cross-sectional area of a groove depends on the conical angle or nose radius of the scratching diamond. The larger the conical angle or nose radius, the larger the cross-sectional area, and vice versa. Hence the pile-up coefficient increased with increasing conical angle or nose radius.

3.3. Subsurface damage

Fig. 11 showed grooves beneath which there existed some cracks. These cracks can be divided into two kinds as follows.

One kind is a microcrack cluster which looks very

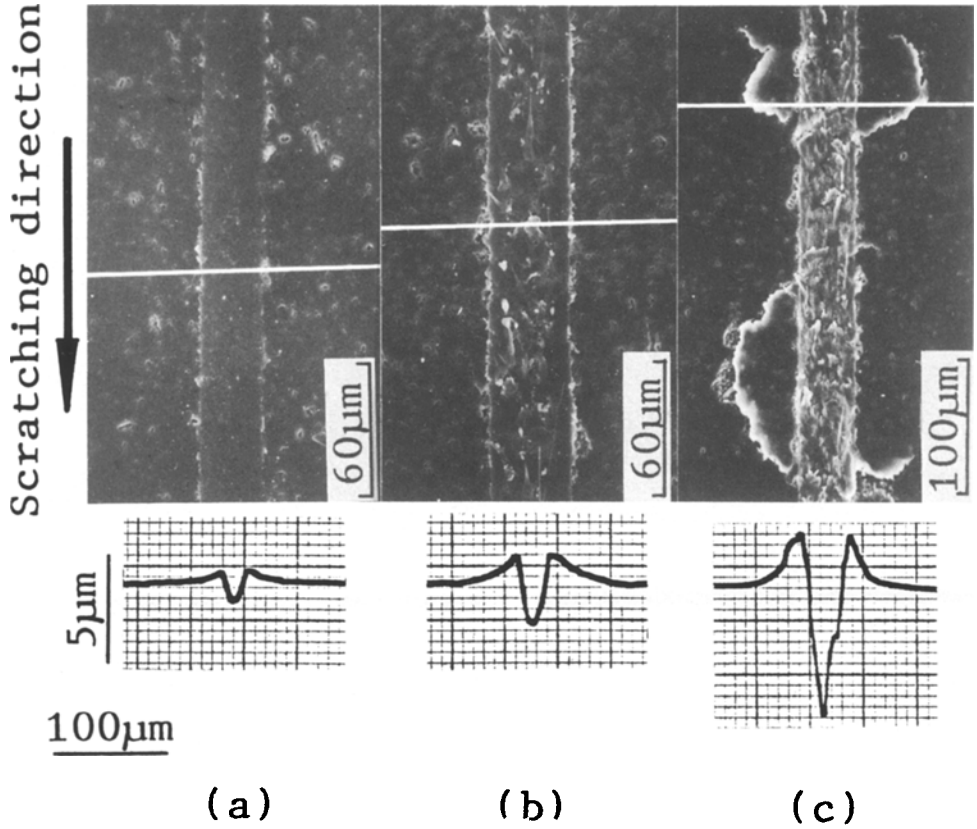

Figure 10 SEM observations and transverse profiles of the grooves scratched by Diamond No. 4 at (a) 1 μm, (b) 2.5 μm and (c) 7.5 μm. White lines indicate measuring routes.

coarse and will be expressed by the symbol I. Fig. 13 shows a cross-section of a groove which was finally taper-polished with 1 μm diamond paste. The diamond tip was transcribed to the sample surface very well. One cannot expect any cracking or chipping on the groove surface except macroscopic plastic deformation, but beneath the groove the microstructure of the material became very loose and many of the grains in the sample fell off during the polishing process.

Another kind is the macrocrack (abbreviated as "crack") which will be represented by the symbol II. This kind of crack usually originated from the boundary of a microcrack cluster and progressed radically. Fig. 14 shows the damage state in the subsurface region of the scratched grooves. With the help of the SEM, the relations between subsurface cracks and the depth of cut or the shape of the diamonds have been made clear.

According to Fig. 14, the penetration zone of the subsurface cracks is described by a half-ellipse. In drawing this half-ellipse, the maximum length of the cracks penetrating towards the inside of the sample will be represented by a and the maximum length of penetration in the transverse direction by b.

3.3.1. Macrocracking

Based on the evaluation method proposed in Fig. 14, variations of a and b with the depth of cut are shown in Figs 15 and 16 for each diamond. The values of either a or b increased with increasing conical angle of the diamond, but the case of the large nose-radius Diamond No. 4 was much different from the cases of the other diamonds. In particular, in the latter cases the values of a and b did not show an evident increase while the depth of cut was small, and rose rapidly as the depth of cut became larger than certain values. For Diamond Nos 1, 2 and 3 these values were approximately 3.5, 3.2 and 2.0 μm, respectively, With Diamond

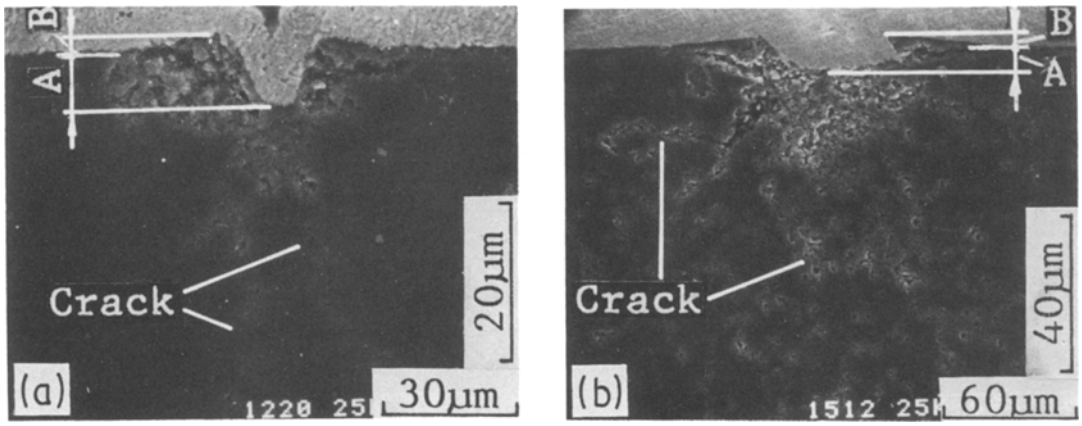

Figure 11 Subsurface damage and surface pile-up induced by (a) No. 2 and (b) No. 4 single-point diamonds; depth of cut 8.5 μm.

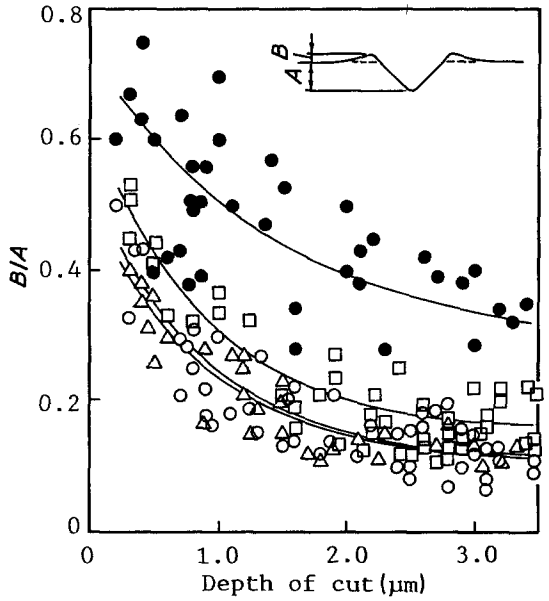

Figure 12 Pile-up coefficient against depth of cut for single-point scratching by different diamonds: (△) No. 1, (○) No. 2, (□) No. 3, (●) No. 4.

No. 4, this gently increasing range did not exist, and the values of a and b rose remarkably from even a very small depth of cut. In the gently increasing range, only microcrack clusters (Type I) were observed in the subsurface region of the scratched groove.

In addition, by comparing Fig. 16 to Fig. 9, it was found that the crack length in the transverse direction on the subsurface was larger than that on the surface, as long as the depth of cut was smaller than 9 μm.

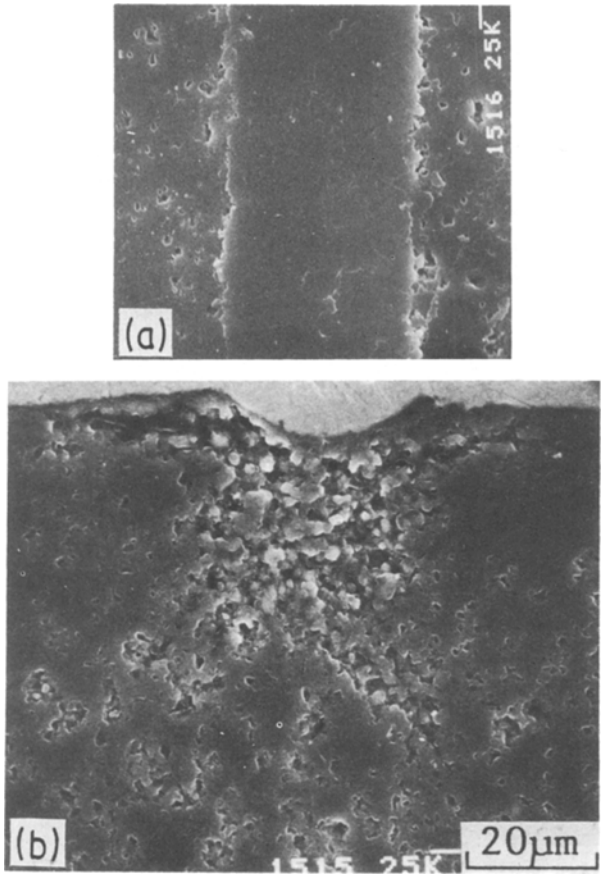

Figure 13 (a) Surface and (b) cross-sectional observations of a smooth groove scratched by Diamond No. 4 at depth of cut 3.8 μm.

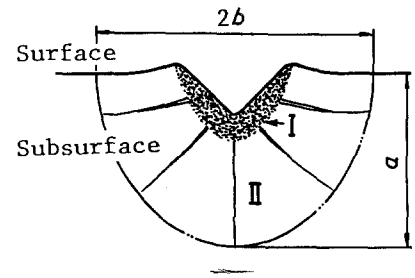

Figure 14 An evaluation method proposed for measuring crack penetration length.

Therefore, it should be said that even though no cracks were observed on the surface, some cracks might have formed in the subsurface layer. When the depth of cut was larger than 9 μm, the crack length on the surface had a tendency to become larger than the one in the subsurface because of surface cracking and chipping or fragmentation.

From Figs 15 and 16, we can expect that the crack lengths will differ greatly if the nose radii of the diamonds differ. In order to illustrate this fact clearly, Fig. 17 gives two SEM photos of the cross-sections of the grooves scratched by Diamond Nos 3 and 4 at the same depth of cut (1.1 μm). There was no macrocrack in the subsurface region when a small nose-radius diamond was used. On the other hand, several macrocracks can be clearly observed in the subsurface layer when a diamond with large nose radius was used.

According to the above results, schematic models are drawn in Fig. 18 which show the half-ellipse-shaped crack zone and macroscopic deformed zone formed by diamonds with large and small nose radii, respectively. If the ratio of crack penetration depth a to depth of cut A is defined as K, then a, as a function of A, can be expressed by

$$a = KA$$

where the proportional ratio K is determined by the

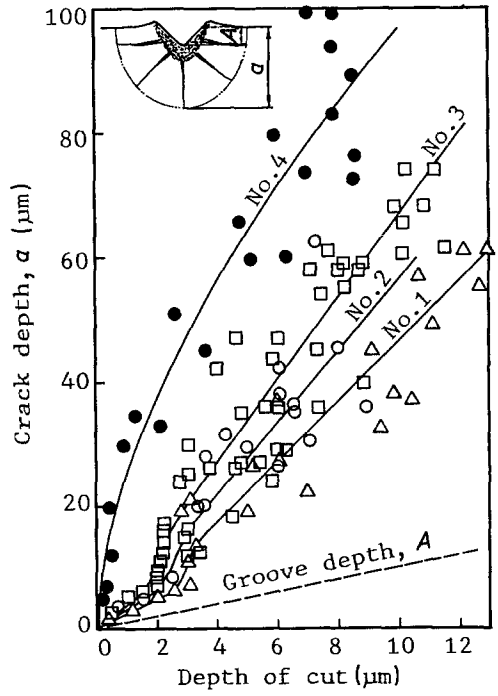

Figure 15 Variations of crack depth a (and groove depth A) with depth of cut for alumina scratched by single-point diamonds.

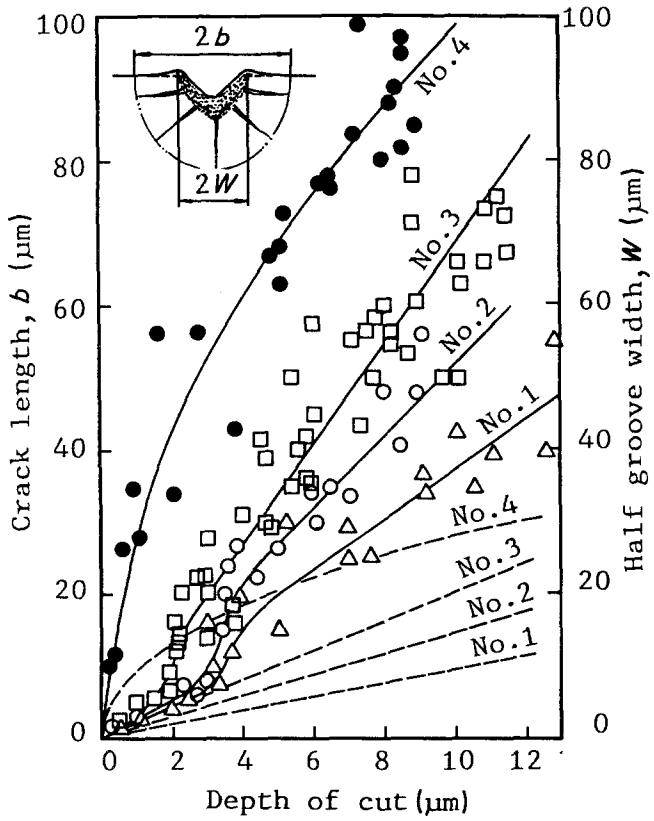

Figure 16 Variations of (——) crack length and (– – –) half groove width with depth of cut for alumina scratched by single-point diamonds.

diamond shape and the depth of cut. Table III gives some values of K which were obtained from the above results. It was noted that when the depth of cut was smaller than 2 μm, the crack depth for the 45 μm nose-radius diamond was almost 8 times that obtained with 1.1 to 1.9 μm diamonds, whereas if the depth of cut was larger than 2 μm, the former was more than twice the latter.

Fig. 19 shows a sectional observation near the corner of a sample. Two grooves which are approximately 5.7 μm in depth lie at the corner about 0.3 mm apart. Beneath the grooves, macrocracks formed and extended not only towards the inside, but also towards the corner of the sample. This is because the constraints on the material near the corner are much weaker than far from the corner. This explains why chipping near the corner is very frequent and sometimes unavoidable.

In order to investigate how the subsurface cracks extend along the scratching direction, the scratched sample was polished parallel to the surface and then observed with the SEM. In Fig. 20, it can be seen that along the scratching direction the cracks extend continuously and form a trunk with the branches spreading away from it.

3.3.2. Microcrack clusters

Fig. 21 shows the fractured surface of a scratched sample and its etched surface. On this fractured surface, microcrack clusters cannot be distinguished from the microstructure even though several macrocracks can be observed distinctly. However, when the fractured surface was etched with 98% H_3PO_4 at 200° C for 17 min, the microcrack cluster was easily removed and the other part of the fractured surface remained almost unchanged.

Fig. 22 gives quantitative results for the microcrack clusters for Diamond Nos 3 and 4. The variations of the removed area $\mathscr{A}$ (which includes the groove area) with depth of cut are shown in this graph. The removed area of the groove scratched by Diamond No. 4 was more than 4 times that removed by Diamond No. 3 when averaged over a wide range of the depth of cut, because of its large nose radius.

Microcrack clusters resulted from the special state of stress applied by a single-point diamond. When

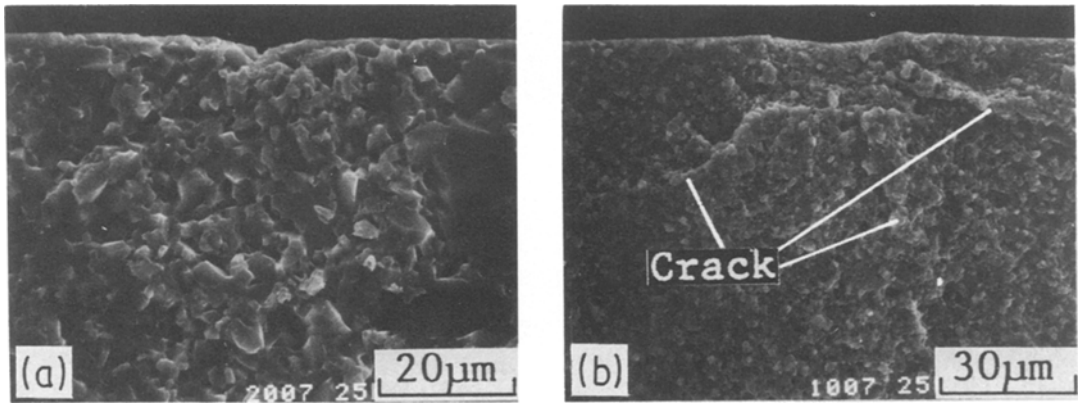

Figure 17 Comparison of the subsurface damage produced by (a) No. 3 and (b) No. 4 diamonds; depth of cut 1.1 μm.

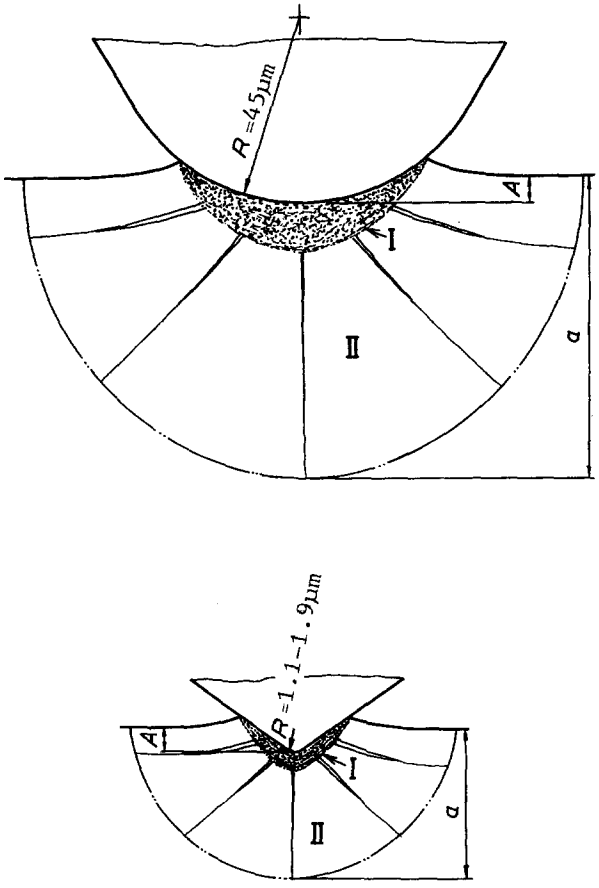

Figure 18 Schematic diagrams of half-ellipse-shaped crack zone and macroscopic deformed zone formed by diamonds with large and small R, respectively.

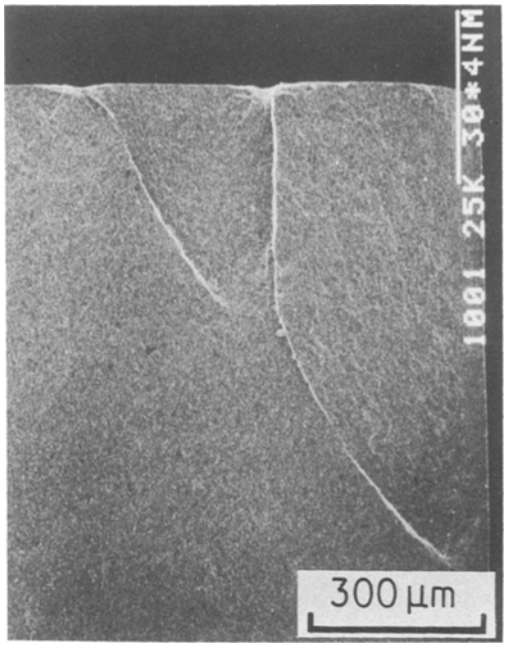

Figure 19 Penetration of macrocracks near the corner of the sample scratched by Diamond No. 4 at depth of cut 5.7 μm.

TABLE III Variations of proportional ratio K with depth of cut

Depth of cut	Diamond nose radius (μm)	
	1.1 to 1.9	45.0
0 to 2	3	23
2~	5.5	13

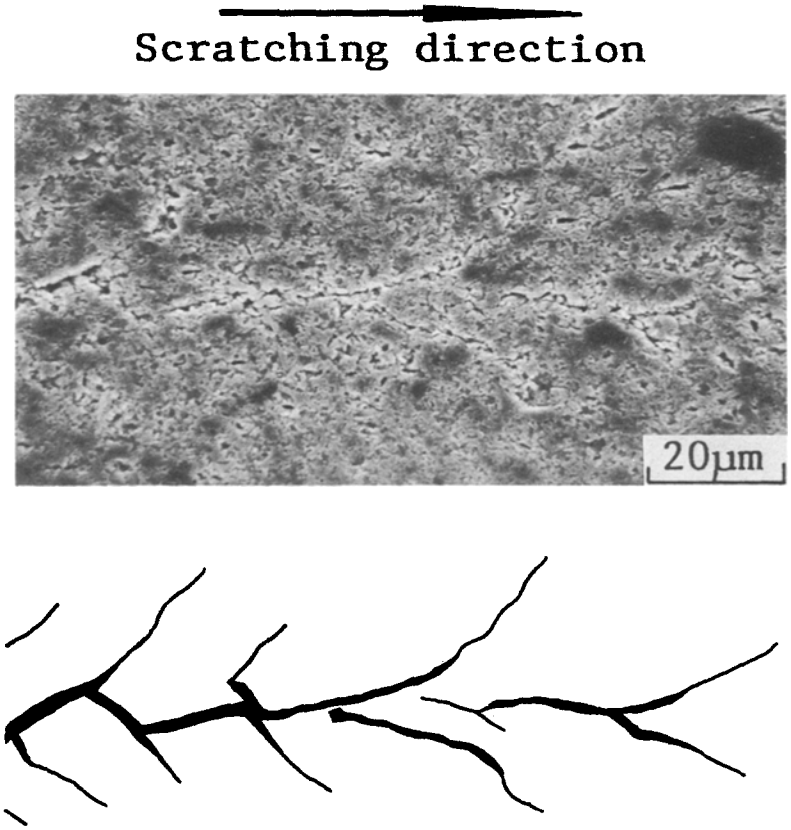

Figure 20 Subsurface crack beneath a 3.5 μm groove scratched by Diamond No. 3; thickness of layer lapped from surface = 7 μm.

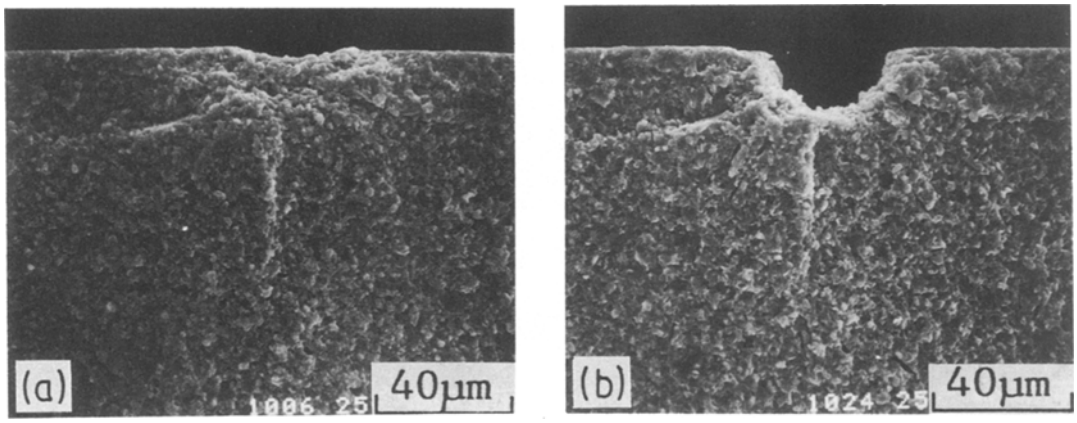

Figure 21 SEM observations of the fractured surface (a) before and (b) after etching. The sample was scratched by Diamond No. 4 at depth of cut 5 μm.

scratching, the stress field on the alumina surface is somewhat similar to a sliding Hertzian stress field with contact friction. One can expect that there is a very strong compression ahead of the diamond, and a very strong tension beneath the groove behind the diamond [1]. Hence the material near the surface is fractured into microcrack clusters by the compression and subsequent tension stresses. A blunt diamond may cause a larger stress field than a sharp one owing to its large nose radius and, therefore, larger friction.

3.4. Cracking mechanisms

Fig. 23 shows scratching models for illustrating the material removal and cracking mechanisms when 1.1 to 1.9 μm diamonds were used. Fig. 23a gives the case of depth of cut smaller than 1 μm. There was almost no material removal, but microcrack clusters formed beneath the groove surface. On the two sides of the groove there existed pile-up because of the transfer of the microcrack clusters.

Fig. 23b is for the case of depth of cut 1 to 3.5 μm. Microcutting may occur, and material removal can be expected. At the same time, stick–slip of the single-point diamond may happen on the groove bottom. For this reason, a scale-like crack forms and the groove surface becomes rough and coarse. The pile-up becomes great due to the larger depth of cut. At this stage, there is still almost no macrocrack nor chipping or fragmentation around or beneath the scratched groove.

Fig. 23c is for a depth of cut more than 3.5 μm. Cracks or chipping form and then develop, and a large amount of material may be removed because of the larger depth of cut. Furthermore, another sort of material removal may be expected by large-scale chipping or fragmentation around the etched groove. Because the macrocrack originates and develops towards the inside of the material, it greatly weakens the material.

The cracking mechanism caused by a diamond with large nose radius is almost the same as that in Fig. 23c, even if the depth of cut is very small.

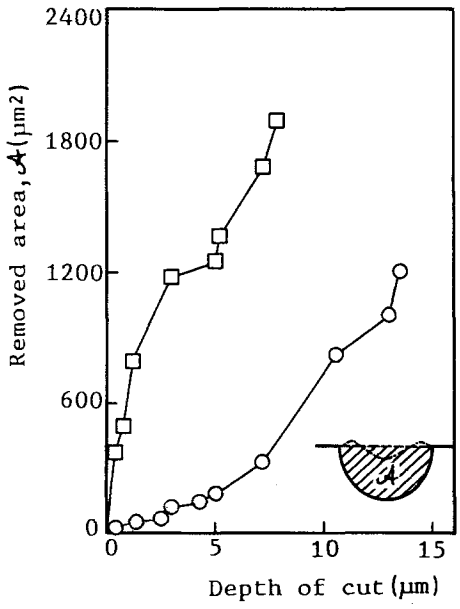

Figure 22 Variations of microcrack cluster area with depth of cut for diamond scratching: (○) R = 1.9 μm (No. 3), (□) R = 45 μm (No. 4).

4. Conclusions

Scratching experiments have been carried out on hot-pressed alumina ceramics by using single-point diamonds with nose radii 1.1 to 45 μm. Cracking and material removal mechanisms have been proposed.

Using diamonds with 1.1 to 1.9 μm nose radius, with depth of cut less than 1 μm, there is almost no material removal but there is microcrack cluster formation beneath the scratched groove. Microcrack clusters play an important role in producing the pile-up on two sides of the groove. For a depth of cut 1 to 3.5 μm microcutting occurs, and material may be removed to some extent. Scale-like cracks form on the groove bottom. For a depth of cut more than 3.5 μm, a macrocrack originates and spreads towards the inside of the material. Large amounts of material may be removed.

In addition, with a 45 μm diamond the macrocrack forms even at very small depths of cut. When the depth of cut is less than 2 μm, the penetration length of the macrocrack caused by a 45 μm diamond is almost 8 times as large as that caused by 1.1 to 1.9 μm diamonds; however, for a depth of cut more than 2 μm the former is more than twice as large as the latter.

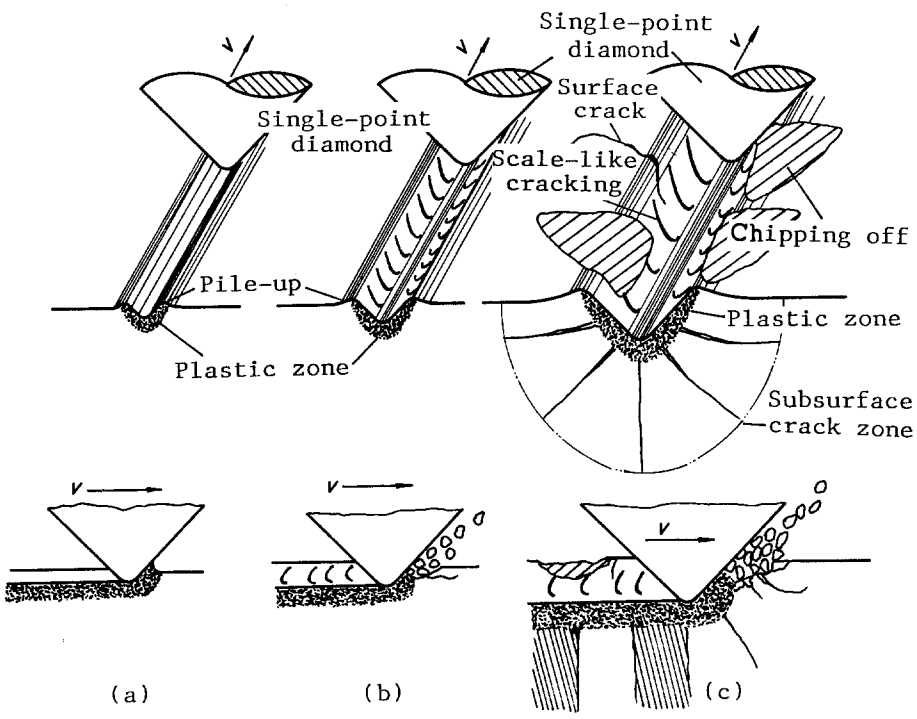

Figure 23 (a–c) Scratching models for illustrating alumina material removal and cracking mechanisms.

References

1. M. V. SWAIN, *Proc. R. Soc.* **A336** (1979) 575.
2. H. P. KIRCHNER and E. D. ISSACSON, *J. Amer. Ceram. Soc.* **65** (1982) 55.
3. H. P. KIRCHNER, *ibid.* **67** (1984) 127.
4. *Idem, ibid.* **67** (1984) 347.
5. H. P. KIRCHNER, R. M. GRUVER and D. M. RICHARD, in "The Science of Ceramic Machining and Surface Finishing II", edited by B. J. Hockey and R. W. Rice, NBS Special Publication No. 562 (National Bureau of Standards, Washington, DC, 1979) p. 23.
6. O. IMANAKA, S. FUJINO and S. MINETA, in "The Science of Ceramic Machining and Surface Finishing I", edited by S. J. Schneider Jr and R. W. Rice, NBS Special Publication No. 348 (National Bureau of Standards, Washington, DC, 1972) p. 37.
7. ZHANG BI, H. TOKURA and M. YOSHIKAWA, *J. Jpn Soc. Precis. Eng.* **52** (1986) 731.

Received 7 September
and accepted 10 December 1987